J. Fluid Mech. (1986), *vol.* 164, *pp.* 127–154
Printed in Great Britain

Weakly nonlinear acoustic and shock-wave theory of the noise of advanced high-speed turbopropellers

By CHRISTOPHER K. W. TAM
Department of Mathematics, Florida State University, Tallahassee, Florida 32306
AND M. SALIKUDDIN
Lockheed-Georgia Company, Marietta, Georgia 30063

(Received 18 October 1984 and in revised form 30 July 1985)

An acoustic and shock-wave theory of the noise generated by advanced turbopropellers operating at supersonic tip helical velocity and high-subsonic cruise Mach number is developed. The theory includes the thickness and loading noise of the highly swept propeller blades. When operating at their design conditions these propellers radiate extremely intense sound waves. Because of the weakly nonlinear propagation effects these high-intensity acoustic disturbances steepen up quickly to form shock waves. In the present theory advantage is taken of the fact that in the blade fixed-rotating-coordinate system the acoustic and shock-wave fields are time independent. The problem is formulated in this coordinate system as a boundary-value problem. Weakly nonlinear propagation effects are incorporated into the solution following Whitham's nonlinearization procedure (Whitham 1974). The change in the disturbance-propagation velocity due to fluid-particle motion as well as the change in the speed of sound resulting from compression and rarefaction are all taken into account. It is found that the equal-area rule of Whitham's shock-fitting method is also applicable to the present problem. This method permits easy construction of the three-dimensional shock surfaces associated with the acoustic disturbances of these high-speed turbopropellers. Numerical results of the present theory are compared with the measurements of the JETSTAR flight experiment and the United Technology Research Center low-cruise Mach number open-wind-tunnel data. Very favourable overall agreements are found. The comparisons indicate clearly that, when these supersonic turbopropellers are operated at their high subsonic design-cruise Mach number, weakly nonlinear propagation effects must be included in the theory if an accurate prediction of the waveform of the sound wave incident on the design aircraft fuselage is to be obtained. This is especially true for noise radiated in the upstream or forward directions. In the forward directions the effective propagation velocity of the acoustic disturbances is greatly reduced by the convection velocity of the ambient flow. This allows more time for the cumulative nonlinear propagation effects to exert their influence, leading to severe distortion of the waveform and the formation of shock waves.

1. Introduction

In recent years, it has been demonstrated, e.g. Dugan *et al.* (1980), that high-speed turbopropellers (propfans) offer a significantly higher propulsive efficiency compared to that of the high-bypass-ratio turbofan engines used to power the present generation of commercial aircraft. However, before the potential fuel savings

associated with the high-speed turbopropellers can be realized in practice in future aircraft designs, several important technological problems must first be solved. One of the more serious problems is the noise generated by these turbopropellers. Because these propellers are to be operated at supersonic blade-tip helical velocity they tend to generate intense noise. This could lead to unacceptable levels of discomfort inside the aircraft cabin.

The objective of this work is to develop a theory to calculate the noise field generated by these advanced turbopropellers. This theory will include weakly nonlinear propagation effects and shock waves.

The blades of advanced turbopropellers are very thin. For the SR-3 propfan under consideration by NASA the blade-thickness to chord ratio is less than 4% over the entire length of the outer half of the blades. One very important consequence of using very thin blades is that the flow field in the immediate neighbourhood of the propeller is probably linear. Unlike previous-generation propellers the blades of advanced turbopropellers are not straight. Instead they have considerable sweep as shown in figure 1. The sweep of the blades provides good aerodynamic performance as well as excellent noise reduction characteristics (see e.g. Metzger & Rohrbach 1979; Hanson 1980*b*). Owing to the sweep, pressure disturbances generated by different parts of the blade are slightly out of phase. When these disturbances arrive at an observer they will, therefore, tend to cancel each other, leading to significant reduction in the noise intensity.

At the present time, several theories are available in the open literature for the calculation of the noise associated with advanced turbopropellers, e.g. Hanson (1980*a*, *b*), Woan & Gregorek (1978), Jou (1979), Farassat (1975, 1981), Nystrom & Farassat (1980), Farassat & Succi (1980). However, all of these are linear theories. Although they differ substantially in the procedure of computation (time-domain versus frequency-domain calculation) they are all based on the acoustic-analogy formulation first used by Lighthill (1952). Lighthill developed the acoustic-analogy theory for the purpose of estimating the noise generated by turbulence in jets (see also Goldstein 1976). The idea was extended formally to sound generation by solid surfaces in motion by Ffowcs Williams & Hawkings (1969). Within the framework of the 'acoustic analogy' of Lighthill and its extensions by others, all the nonlinear effects are lumped together into the quadrupole terms. These quadrupole terms are to be treated as inhomogeneous terms of the linear wave equation. Thus external input is needed to determine the effects of nonlinearity. The usual practice is to make an independent nonlinear calculation to estimate these terms. Then the quadrupole terms are used as source terms to calculate the acoustic field.

For the advanced-turbopropeller-noise problem important nonlinear effects can arise in two ways. First, if the flow field around the propeller is significantly disturbed by the moving blades then nonlinear effects must be taken into consideration in calculating the loading on the blade, and its associated radiation field. Second, even if the blades do not significantly disturb the flow, different parts of the disturbance would propagate with different velocities due to the slight change in the speed of sound under compression or rarefaction and different fluid-particle velocities. This effect when accumulated over some distance would severely distort the waveform of the disturbance, leading to the formation of shock waves. This weakly nonlinear propagation effect is well known in sonic-boom problems. Hanson & Fink (1979) used the acoustic-analogy theory to estimate the effect of nonlinearities on the acoustic field. They found that for thin blades such as those used for propfans the quadrupole terms are relatively unimportant. However, it must be pointed out that their estimate

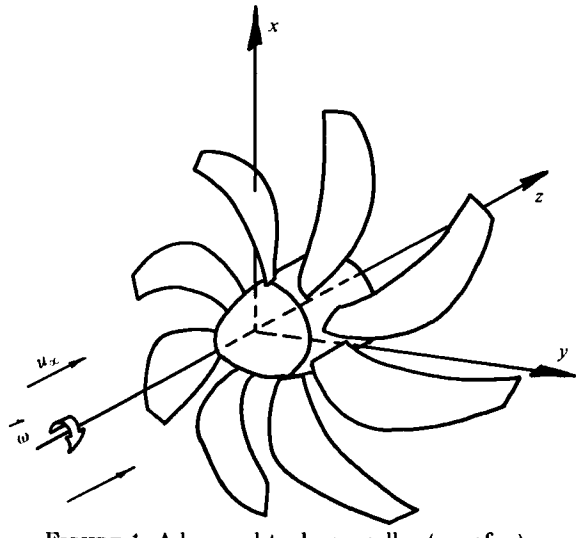

FIGURE 1. Advanced turbopropeller (propfan).

is strictly confined to the nonlinearity of the flow field in the immediate neighbourhood of the blades. On the other hand recent flight measurements of the acoustic disturbances generated by the advanced turbopropellers indicate the presence of shock waves in the pressure waveform (see figure 12, also Brooks 1983). These shock waves are, therefore, most probably developed as a consequence of weakly nonlinear propagation effects. These effects have not been accounted for in all the turbopropeller-noise theories currently available in the literature.

One of the most severe drawbacks of the theories based on the acoustic-analogy approach is that external input is needed to determine the effect of nonlinearity. In the case of nonlinear propagation effects, the necessary input requires knowledge of the nonlinear solution. Of course, if one knows the nonlinear solution already there is no need to redetermine it through the acoustic analogy. Hence it is fair to say that there is no self-consistent way of calculating the nonlinear propagation effects by the theories predicated on the acoustic analogy of Lighthill and others. More recently Tam & Burton (1984) succeeded in developing a supersonic-jet-noise theory starting from the equations of motion of a compressible fluid without the use of the acoustic analogy and the concept of quadrupoles. Thus it appears that even in the case of the jet-noise problem the use of the acoustic-analogy approach is not only not necessary but also possibly not even appropriate.

In this paper, the problem of the acoustic field generated by a supersonic turbopropeller is formulated and solved as a boundary-value problem with the equations of motion of an inviscid compressible fluid as the governing equations. To facilitate the solution of the problem a blade-fixed cylindrical coordinate system is used. In this (rotating) blade-fixed-coordinate system the disturbance field is time independent so that the solution is a function of the spatial coordinates alone. To simplify the problem further, the thin-airfoil approximation is adopted. This approximation allows the boundary conditions to be prescribed on the mean-blade surface instead of the actual surface of the blade. This approximation is justified since the thickness-to-chord ratios of the blades of advanced turbopropellers are, indeed, very small. Because these turbopropellers have high sweep and very thin blades, nonlinear effects of the flow field in the immediate neighbourhood of the propellers

are known to be relatively unimportant. In this work, therefore, only the linearized boundary-value problems corresponding to the thickness noise and the loading noise are solved in the blade-fixed-coordinate system.

The linear thickness- and loading-noise problems of advanced turbopropellers, as mentioned before, have been solved previously by a number of investigators. Explicit near- and far-field solutions have recently been given by Hanson (1985) in retarded coordinates. Hanson developed these solutions by the acoustic-analogy theory. For the purpose of calculating the linear sound field the use of the acoustic-analogy theory and the retarded coordinates appear to provide numerical results identical with the present approach involving the solution of the equations of motion of an inviscid compressible fluid in a blade-fixed-coordinate system. Significant differences arise, however, when weakly nonlinear effects are to be accounted for. In the acoustic-analogy theory these effects are, in principle, lumped into the quadrupole terms and are therefore difficult, if not impossible, to recover. Moreover, it is found that, if three-dimensional weak shocks are to be added to the solution, the shock-fitting procedure can be carried out most efficiently (or is practical) only if a blade-fixed-coordinate system is used.

To incorporate the weakly nonlinear propagation effects on the linear solution, Whitham's nonlinearization procedure is employed (Whitham 1974, chapter 9). The change in disturbance-propagation velocity due to fluid-particle motion as well as the change in the speed of sound resulting from compression and rarefaction are all taken into account. The nonlinearized solution causes the waveform to steepen in the compression phase of the acoustic wave. This process leads to the formation of weak shocks. It is shown that the equal-area rule of Whitham's shock-fitting method is applicable to the present problem. By carrying out these procedures in the blade-fixed-coordinate system the three-dimensional shock surfaces associated with the acoustic field of an advanced turbopropeller are constructed.

Prior to the present work Hawkings & Lowson (1974) investigated the weakly nonlinear steepening effects of sound generated by an open supersonic rotor. Later Barger (1980) considered the general case of a rotor moving with a constant forward velocity. In Barger's analysis, however, the choice of coordinate system is such that the sound-field pattern is unsteady so that the cumbersome procedure of determining the ray-tube areas must be carried out before the shock-fitting process can be applied. Because of this the construction of the three-dimensional shock surfaces associated with each propeller blade becomes extremely difficult and complicated. In the present approach such difficulty is totally eliminated by the use of the blade-fixed-coordinate system.

Numerical results for the noise of the SR-3 turbopropeller are presented in §6. The calculated pressure waveforms at the design-cruise condition (cruise Mach number $= 0.8$) are compared with the flight measurements of the JETSTAR program. Very favourable agreements are found. Additional comparisons between calculated results and experimental waveforms measured in the United Technology Research Center open wind-tunnel facility have also been carried out. Since the open wind tunnel can only be run at low subsonic speed (Mach number $\leqslant 0.323$) the turbopropeller was operated at an off-design environment in these tests. The agreement between the theoretical results and measurements is again found to be quite good. However, the weakly nonlinear propagation effects are less significant at this off-design operating condition. The importance of nonlinear propagation effects at the design-cruise Mach number is evaluated by examining the shock-formation distance as a function of the direction of propagation. Nonlinear distortion of the waveform in selected directions

is presented. The time history as well as the propagation of weak shocks and the subsequent evolution of the waveform as a function of radial distance from the turbopropeller are described. It is found that nonlinear propagation effects are especially important for noise radiation in the upstream or forward direction. Significant distortion of the waveform occurs over the first few diameters from the turbopropeller. A physical explanation of this finding is provided at the end of the paper.

2. Formulation

Consider a coordinate system (x, y, z) the z-axis of which coincides with the axis of the turbopropeller as shown in figure 1. This coordinate sytem is stationary relative to the wing and fuselage of the aircraft on which the turbopropeller is mounted. In this coordinate system the linearized equations of motion of an inviscid compressible fluid are

$$\frac{\partial \rho}{\partial t} + U_\infty \frac{\partial \rho}{\partial z} + \rho_\infty \nabla \cdot \boldsymbol{v} = 0, \tag{2.1}$$

$$\rho_\infty \left(\frac{\partial \boldsymbol{v}}{\partial t} + U_\infty \frac{\partial \boldsymbol{v}}{\partial z} \right) = -\nabla p, \tag{2.2}$$

$$p = a_\infty^2 \rho.$$

Equations (2.1) and (2.2) are the linearized continuity and momentum equations. Here ρ, $\boldsymbol{v}$ and p are the perturbation density, velocity and pressure, respectively. U_∞, ρ_∞ and a_∞ are the cruise velocity of the aircraft, the ambient density and the speed of sound of the fluid. For irrotational fluid motion the velocity field can be expressed in terms of a velocity potential Φ defined by

$$\boldsymbol{v} = \nabla \Phi. \tag{2.3}$$

Substitution of (2.3) into (2.2) gives the following relationship between p, the pressure, and Φ,

$$p = -\rho_\infty \left(\frac{\partial \Phi}{\partial t} + U_\infty \frac{\partial \Phi}{\partial z} \right). \tag{2.4}$$

On eliminating the density ρ in (2.1) by means of the isentropic relation $p = a_\infty^2 \rho$ and p by (2.4), a single equation for Φ is found,

$$\nabla^2 \Phi - \frac{1}{a_\infty^2} \left(\frac{\partial}{\partial t} + U_\infty \frac{\partial}{\partial z} \right)^2 \Phi = 0. \tag{2.5}$$

Equation (2.5) will be used for the determination of the acoustic field associated with the thickness distribution of the blade. This is often referred to as the 'thickness noise'. To calculate the noise field associated with the loading on the blade it would be more convenient to use p, the pressure, as the dependent variable. The governing equation for p is obtained by differentiating equation (2.5) by $(\partial/\partial t) + U_\infty(\partial/\partial z)$. Upon using equation (2.4) it is easy to find that p satisfies the same equation as Φ, i.e.

$$\nabla^2 p - \frac{1}{a_\infty^2} \left(\frac{\partial}{\partial t} + U_\infty \frac{\partial}{\partial z} \right)^2 p = 0. \tag{2.6}$$

To calculate the radiated acoustic field it is advantageous to rewrite (2.5) and (2.6) in a blade-fixed (rotating) coordinate system. Let (r, θ_s, z) be the cylindrical

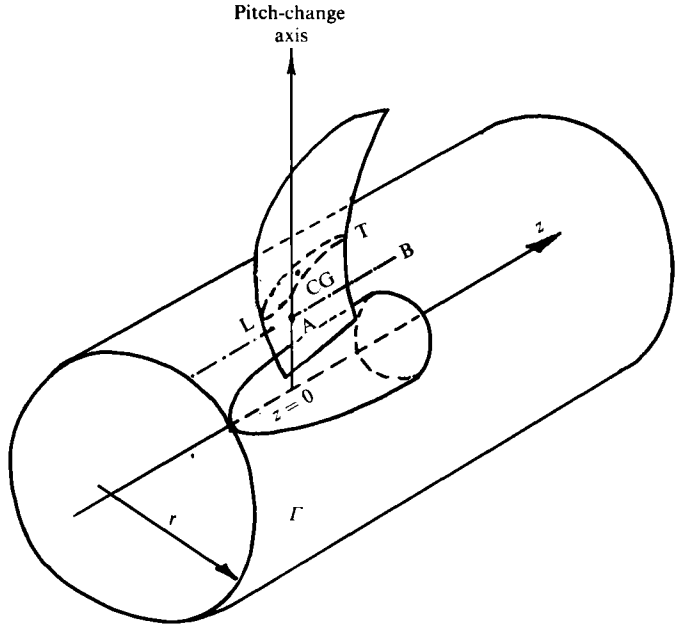

FIGURE 2. Schematic drawing showing the pitch-change axis of the mth blade and the intersection of the blade and the cylindrical surface Γ.

coordinates of the stationary-coordinate system and (r, θ, z) be those of the blade-fixed-coordinate system. If $\boldsymbol{\omega} = \omega \hat{e}_z$ ($\hat{e}_z$ is the unit vector in the z-direction) is the angular velocity of the propeller (see figure 1) then

$$\theta = \theta_s - \omega t. \tag{2.7}$$

In the blade-fixed-coordinate system all physical quantities of the flow are time-independent or functions of (r, θ, z) alone. Thus on using (2.7) it is straightforward to derive the following transformation of derivatives

$$\frac{\partial}{\partial t} \to -\omega \frac{\partial}{\partial \theta}, \quad \frac{\partial}{\partial \theta_s} \to \frac{\partial}{\partial \theta}. \tag{2.8a, b}$$

By means of the above transformation, (2.5) and (2.6) may be written as

$$\left(\frac{\partial^2}{\partial r^2} + \frac{1}{r}\frac{\partial}{\partial r} + \frac{1}{r^2}\frac{\partial^2}{\partial \theta^2} + \frac{\partial^2}{\partial z^2}\right)\begin{pmatrix}\Phi \\ p\end{pmatrix} - \frac{1}{a_\infty^2}\left(U_\infty \frac{\partial}{\partial z} - \omega \frac{\partial}{\partial \theta}\right)^2 \begin{pmatrix}\Phi \\ p\end{pmatrix} = 0. \tag{2.9a, b}$$

2.1. *Blade geometry and local coordinates*

For convenience of prescribing boundary conditions on the surface of the blades, a set of local coordinates is adopted. Consider the mth blade of the turbopropeller as shown in figure 2. Let Γ be the curved surface of the circular cylinder of radius r. The thickness distribution of the blade is prescribed on the intersection of surface Γ and the blade. This is shown in figure 3. Figure 3 is essentially surface Γ laid flat on a plane parallel to the z-axis and perpendicular to the pitch-change axis at $z = 0$. The velocity diagram of the incoming flow as seen by the blade on surface Γ is also given in this figure. The incoming undisturbed velocity has a velocity vector equal to $U_\infty \hat{e}_z - \omega r \hat{e}_\theta$, where $\hat{e}_z$ and $\hat{e}_\theta$ are unit vectors in the z- and θ-directions. To describe the geometry of the mth blade a set of local coordinates (r, ξ_m, ζ_m) as shown in figure 3 are used. The origin of the ξ_m and ζ_m coordinates is at a distance $\eta(r)$ from the

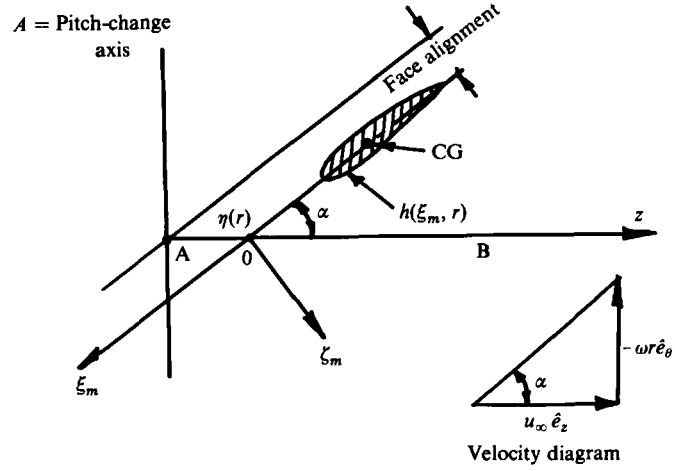

FIGURE 3. Local coordinates (r, ξ_m, ζ_m) on surface Γ.

pitch-change axis of the blade. These local coordinates are related to the blade-fixed cylindrical coordinates (r, θ, z) by

$$\left.\begin{aligned} \theta - \theta_m &= \left(\omega\xi_m + \frac{U_\infty \zeta_m}{r}\right)\frac{1}{(U_\infty^2 + \omega^2 r^2)^{\frac{1}{2}}} \\ z &= \frac{(-U_\infty \xi_m + \omega r \zeta_m)}{(U_\infty^2 + \omega^2 r^2)^{\frac{1}{2}}} + \eta \end{aligned}\right\} \quad (r = r), \tag{2.10}$$

or

$$\left.\begin{aligned} \zeta_m &= [z\omega + (\theta - \theta_m)\, U_\infty - \eta\omega]\frac{r}{(U_\infty^2 + \omega^2 r^2)^{\frac{1}{2}}} \\ \xi_m &= [-zU_\infty + r^2(\theta - \theta_m)\,\omega + \eta U_\infty]\frac{1}{(U_\infty^2 + \omega^2 r^2)^{\frac{1}{2}}} \end{aligned}\right\} \quad (r = r). \tag{2.11}$$

In the above equations, θ_m is the θ-coordinate of the pitch-change axis of the mth blade and $\eta(r)$ is related to the face alignment of the blades. The face alignment is usually very small and changes extremely slowly in the radial direction. For the SR-3 turbopropeller it is very small. For simplicity, it will be set equal to zero in the calculation. In what follows it will be assumed that $\mathrm{d}\eta/\mathrm{d}r$ is small (i.e. $\mathrm{d}\eta/\mathrm{d}r \ll 1$; this is true in practice) and can be neglected as a first approximation. Now if (2.9) is rewritten in terms of the local coordinates (r, ξ_m, ζ_m), the left-hand side becomes

$$\begin{aligned} &\nabla^2\begin{bmatrix}\Phi\\ p\end{bmatrix} - \frac{1}{a_\infty^2}\left(U_\infty\frac{\partial}{\partial z} - \omega\frac{\partial}{\partial\theta}\right)^2\begin{bmatrix}\Phi\\ p\end{bmatrix} \\ &= \left\{\frac{\partial^2}{\partial r^2} + \left[1 + \frac{U_\infty^4\,\zeta_m^2}{r^2(U_\infty^2 + \omega^2 r^2)^2}\right]\frac{\partial^2}{\partial\zeta_m^2} + \left[1 + \frac{(2U_\infty\omega\zeta_m + \omega^2 r\xi_m)^2}{(U_\infty^2 + \omega^2 r^2)^2} - \frac{U_\infty^2 + \omega^2 r^2}{a_\infty^2}\right]\frac{\partial^2}{\partial\xi_m^2}\right. \\ &\quad + \frac{2U_\infty^2\,\zeta_m}{r(U_\infty^2 + \omega^2 r^2)}\frac{\partial^2}{\partial\zeta_m\,\partial r} + \frac{2(2U_\infty\omega\zeta_m + \omega^2 r\xi_m)}{U_\infty^2 + \omega^2 r^2}\frac{\partial^2}{\partial\xi_m\,\partial r} \\ &\quad + 2U_\infty^2\,\zeta_m\frac{2U_\infty\omega\zeta_m + \omega^2 r\xi_m}{r(U_\infty^2 + \omega^2 r^2)^2}\frac{\partial^2}{\partial\zeta_m\,\partial\xi_m} + \frac{1}{r}\frac{\partial}{\partial r} + \frac{U_\infty^2(U_\infty^2 - 2\omega^2 r^2)\,\zeta_m}{r^2(U_\infty^2 + \omega^2 r^2)^2}\frac{\partial}{\partial\zeta_m} \\ &\quad \left. + \frac{4U_\infty^3\,\omega\zeta_m + (2U_\infty^2 + \omega^2 r^2)\,\omega^2 r\xi_m}{r(U_\infty^2 + \omega^2 r^2)^2}\frac{\partial}{\partial\xi_m}\right\}\begin{bmatrix}\Phi\\ p\end{bmatrix} = 0. \end{aligned} \tag{2.12a, b}$$

This form of (2.9) will be useful later on.

2.2. *Boundary-value problem for the thickness noise*

Within the framework of the thin-airfoil approximation, each blade of the turbopropeller can be replaced by a thickness distribution (sources and sinks) and a loading distribution on the mean blade surface $\zeta_m = 0$. To linear order the noise associated with the thickness distribution and that of the loading distribution are uncoupled so that they can be solved separately.

Let us first consider the thickness-noise problem. In this case the thickness of the blade is taken to be distributed symmetrically about the mean blade surface $\zeta_m = 0$. Now the boundary condition on the turbopropeller requires that the relative velocity component normal to the surface of the blade be equal to zero. If $h(\xi_m, r)$ denotes the thickness distribution of the blade (see figure 3), then this boundary condition when expressed mathematically gives

$$(U_\infty \hat{e}_z - \omega r \hat{e}_\theta + \nabla\Phi)\cdot\nabla(\zeta_m \pm h(\xi_m, r)) = 0 \quad \text{as} \quad \zeta_m \to 0^\pm. \tag{2.13}$$

Within the thin-airfoil approximation it is permissible to satisfy boundary condition (2.13) on the mean blade surface $\zeta_m = 0$ instead of the actual blade surface as is indicated. On retaining linear-order terms only it is easy to show that (2.13) simplifies to

$$\frac{\partial\Phi}{\partial\zeta_m} = \mp(U_\infty^2 + \omega^2 r^2)^{\frac{1}{2}} \frac{\partial h}{\partial\xi_m} \quad \text{as} \quad \zeta_m \to 0^\pm. \tag{2.14}$$

In other words $\partial\Phi/\partial\zeta_m$ has a discontinuity or jump at the mean blade surface. This jump condition may be rewritten as

$$\lim_{\epsilon\to 0}\left[\frac{\partial\Phi}{\partial\zeta_m}\right]_{\zeta_m=-\epsilon}^{\zeta_m=\epsilon} = -2(U_\infty^2 + \omega^2 r^2)^{\frac{1}{2}} \frac{\partial h}{\partial\xi_m}. \tag{2.15}$$

The thickness-noise problem, therefore, consists of finding a solution to equation (2.9*a*) and the jump condition (2.15) for $m = 1, 2, 3, \ldots, B$, where B is the total number of blades. Equation (2.9*a*) and the jump condition can, however, be cast into a single inhomogeneous equation. It is easy to find that the required inhomogeneous equation is

$$\nabla^2\Phi - \frac{1}{a_\infty^2}\left(U_\infty\frac{\partial}{\partial z} - \omega\frac{\partial}{\partial\theta}\right)^2\Phi = -\sum_{m=1}^{B} 2(U_\infty^2 + \omega^2 r^2)^{\frac{1}{2}} \frac{\partial h}{\partial\xi_m}\delta(\zeta_m), \tag{2.16}$$

where $\delta(\zeta_m)$ is the delta function. To show that (2.16) is the correct equation for the thickness-noise problem, first, it is to be noted that away from the mean blade surfaces this equation is the same as equation (2.9*a*). To recover the jump condition (2.15) one can integrate (2.16) with respect to ζ_m from $\zeta_m = -\epsilon$ to ϵ and let $\epsilon \to 0$. On using the property of the delta function the right-hand side of (2.16) becomes the right-hand side of (2.15) upon integration and taking the limit $\epsilon \to 0$. Next replace the left-hand side of (2.16) by (2.12*a*); upon taking into account the fact that Φ is continuous it is straightforward to find, in the limit $\epsilon \to 0$, all the terms drop out except the second term. This term reproduces the left-hand side of (2.15) and hence the jump condition. Thus to find the acoustic field associated with the blade-thickness distribution it is only necessary to solve (2.16) with boundedness or outgoing wave condition far away from the propeller. Instead of the velocity potential Φ the equation for pressure, p, can be obtained by differentiating (2.16) by $\rho_\infty(U_\infty(\partial/\partial z) - \omega(\partial/\partial\theta))$ and using (2.4),

$$\nabla^2 p - \frac{1}{a_\infty^2}\left(U_\infty\frac{\partial}{\partial z} - \omega\frac{\partial}{\partial\theta}\right)^2 p = \sum_{m=1}^{B} 2\rho_\infty\left(U_\infty\frac{\partial}{\partial z} - \omega\frac{\partial}{\partial\theta}\right)(U_\infty^2 + \omega^2 r^2)^{\frac{1}{2}} \frac{\partial h}{\partial\xi_m}\delta(\zeta_m). \tag{2.17}$$

2.3. *Boundary-value problem for the loading noise*

To calculate the acoustic field generated by the loading on the blades it will be assumed that the pressure difference on the two sides of the blades is known. By the thin-airfoil approximation this may be regarded as a prescribed pressure jump on the mean blade surface $\zeta_m = 0$. That is,

$$\lim_{\epsilon \to 0} [p]_{\zeta_m = -\epsilon}^{\zeta_m = \epsilon} = L(\xi_m, r), \tag{2.18}$$

for $m = 1, 2, 3, \ldots, B$, where $L(\xi_m, r)$ is the given loading distribution on the mth blade. Therefore, the loading-noise problem consists of solving equation (2.9*b*) for p together with jump condition (2.18). Again by introducing the delta function it is possible to incorporate equation (2.9*b*) and jump condition (2.18) into a single inhomogeneous equation, which is

$$\nabla^2 p - \frac{1}{a_\infty^2}\left(U_\infty \frac{\partial}{\partial z} - \omega \frac{\partial}{\partial \theta}\right)^2 p = \sum_{m=1}^{B} \frac{\partial}{\partial \zeta_m} [L(\xi_m, r)\, \delta(\zeta_m)]. \tag{2.19}$$

To show that the solution of (2.19) satisfies jump condition (2.18) it is only necessary to integrate (2.19) twice with respect to ζ_m. The upper and lower limits of the second integration are $\zeta_m = +\epsilon$ and $\zeta_m = -\epsilon$. On using (2.12*b*) and noting that

$$\int \delta(\zeta_m)\, \zeta_m \, \mathrm{d}\zeta_m = 0,$$

it is straightforward to recover pressure-jump condition (2.18) in the limit $\epsilon \to 0$. The construction of the solutions of (2.17) and (2.19) will be carried out in the next section.

3. Linear solution

Both the thickness and the loading-noise problems are governed by an inhomogeneous equation of the form

$$\frac{\partial^2 p}{\partial r^2} + \frac{1}{r}\frac{\partial p}{\partial r} + \frac{1}{r^2}\frac{\partial^2 p}{\partial \theta^2} + \frac{\partial^2 p}{\partial z^2} - \frac{1}{a_\infty^2}\left(U_\infty \frac{\partial}{\partial z} - \omega \frac{\partial}{\partial \theta}\right)^2 p = f(r, \theta, z). \tag{3.1}$$

For the thickness-noise problem the inhomogeneous term on the right-hand side of (3.1) is given by that of (2.17), whereas for the loading noise it is given by the right-hand side of (2.19). Equation (3.1) together with boundedness or outgoing wave condition as $|z|, r \to \infty$ can be solved by first applying Fourier transform to the variable z and then expanding the solution as a Fourier series in θ. In the following the Fourier transform of a function will be denoted by an overbar and the nth Fourier component will be labelled by a subscript n as

$$\bar{p}(r, \theta, k) = \frac{1}{2\pi} \int_{-\infty}^{\infty} p(r, \theta, z)\, \mathrm{e}^{-\mathrm{i}kz}\, \mathrm{d}z, \tag{3.2a}$$

$$p(r, \theta, z) = \int_{-\infty}^{\infty} \bar{p}(r, \theta, k)\, \mathrm{e}^{\mathrm{i}kz}\, \mathrm{d}k, \tag{3.2b}$$

and

$$\bar{p}(r, \theta, k) = \sum_{n=-\infty}^{\infty} \bar{p}_n(r, k)\, \mathrm{e}^{\mathrm{i}n\theta}, \tag{3.3a}$$

$$\bar{p}_n(r, k) = \frac{1}{2\pi} \int_0^{2\pi} \bar{p}(r, \theta, k)\, \mathrm{e}^{-\mathrm{i}n\theta}\, \mathrm{d}\theta. \tag{3.3b}$$

From (3.1) it is straightforward to find

$$\frac{\mathrm{d}^2\bar{p}_n}{\mathrm{d}r^2}+\frac{1}{r}\frac{\mathrm{d}\bar{p}_n}{\mathrm{d}r}-\left[k^2-\frac{(kU_\infty-\omega n)^2}{a_\infty^2}+\frac{n^2}{r^2}\right]\bar{p}_n=\bar{f}_n(r,k). \tag{3.4}$$

Equation (3.4) can be solved by the use of a Green function $G(r,s)$ satisfying the inhomogeneous equation

$$\frac{\mathrm{d}^2G}{\mathrm{d}r^2}+\frac{1}{r}\frac{\mathrm{d}G}{\mathrm{d}r}-\left[k^2-\frac{(kU_\infty-\omega n)^2}{a_\infty^2}+\frac{n^2}{r^2}\right]G=\delta(r-s). \tag{3.5}$$

It is easy to construct the Green function $G(r,s)$ in terms of modified Bessel functions of order n, I_n and K_n:

$$G(r,s)=\begin{cases}-sI_n\left(\left(k^2-\dfrac{(kU_\infty-\omega n)^2}{a_\infty^2}\right)^{\frac{1}{2}}s\right)K_n\left(\left(k^2-\dfrac{(kU_\infty-\omega n)^2}{a_\infty^2}\right)^{\frac{1}{2}}r\right) & (r>s),\\ -sI_n\left(\left(k^2-\dfrac{(kU_\infty-\omega n)^2}{a_\infty^2}\right)^{\frac{1}{2}}r\right)K_n\left(\left(k^2-\dfrac{(kU_\infty-\omega n)^2}{a_\infty^2}\right)^{\frac{1}{2}}s\right) & (r<s).\end{cases} \tag{3.6}$$

To ensure that the boundedness or outgoing wave condition is satisfied as $r\to\infty$ the branch cuts of the square-root function in the arguments of the modified Bessel functions are taken so that

$$-\tfrac{1}{2}\pi\leqslant\arg\left(\left(k^2-\frac{(kU_\infty-\omega n)^2}{a_\infty^2}\right)^{\frac{1}{2}}\right)\leqslant\tfrac{1}{2}\pi, \tag{3.7}$$

in the complex k-plane. The branch points are at

$$k_\pm=\frac{\omega n}{a_\infty}\frac{1}{1\pm M_\infty}, \tag{3.8}$$

where $M_\infty=U_\infty/a_\infty$ is the free-stream or cruise Mach number. The branch cuts together with the k-inversion contour in the complex k-plane are shown in figure 4.

By means of $G(r,s)$ the solution for $\bar{p}_n(r,k)$ in the acoustic radiation field $r>b$; b = length of the turbopropeller blade, is

$$\bar{p}_n(r,k)=-K_n\left(\left(k^2-\frac{(kU_\infty-\omega n)^2}{a_\infty^2}\right)^{\frac{1}{2}}r\right)\mu(n,k)\quad(r>b), \tag{3.8a}$$

where

$$\mu(n,k)=\int_0^b\bar{f}_n(r,k)\,I_n\left(\left(k^2-\frac{(kU_\infty-\omega n)^2}{a_\infty^2}\right)^{\frac{1}{2}}r\right)r\,\mathrm{d}r. \tag{3.8b}$$

Upon inverting the Fourier transform and summing over the Fourier components the solution of (3.1) is found to be

$$p(r,\theta,z)=-\sum_{n=-\infty}^{\infty}\int_{-\infty}^{\infty}K_n\left(\left(k^2-\frac{(kU_\infty-\omega n)^2}{a_\infty^2}\right)^{\frac{1}{2}}r\right)\mu(n,k)\,\mathrm{e}^{\mathrm{i}n\theta+\mathrm{i}kz}\,\mathrm{d}k. \tag{3.9}$$

In the acoustic far field, (3.9) can be further simplified. Let (R,χ,θ) be the spherical polar coordinate of a coordinate system whose polar axis coincides with the z-axis. These coordinates are related to (r,θ,z) by

$$z=R\cos\chi.\quad r=R\sin\chi\quad(\theta=\theta).$$

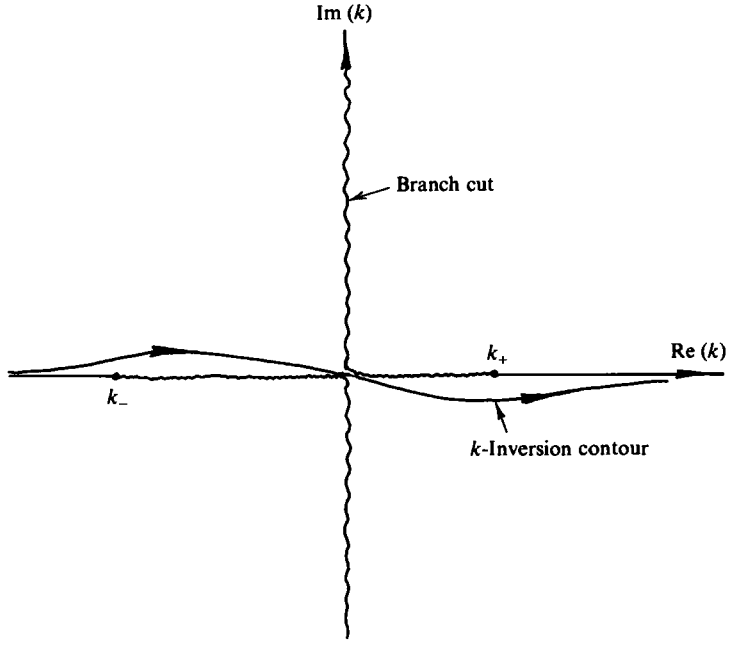

FIGURE 4. The complex k-plane showing branch cuts and the k-inversion contour.

Substitution of the above into (3.9) and using the asymptotic form of the modified Bessel function it is easy to find

$$p(R,\chi,\theta) \sim -\sum_{n=-\infty}^{\infty} \int_{-\infty}^{\infty} \left(\frac{\pi}{2R\sin\chi}\right)^{\frac{1}{2}} \times \frac{\exp\left\{\left[-\left(k^2-\frac{(kU_\infty-\omega n)^2}{a_\infty^2}\right)^{\frac{1}{2}}\sin\chi + ik\cos\chi\right]R + in\theta\right\}\mu(n,k)\,\mathrm{d}k}{\left(k^2-\frac{(kU_\infty-\omega n)^2}{a_\infty^2}\right)^{\frac{1}{4}}} \quad (R \gg b). \tag{3.10}$$

The k-integral in (3.10) can now be evaluated asymptotically by the method of stationary phase. This gives

$$p(R,\chi,\theta) = \frac{1}{R}F\left(\frac{\omega R}{v(\chi)}+\theta,\chi\right) \quad (R \gg b), \tag{3.11a}$$

where

$$F\left(\frac{\omega R}{v(\chi)}+\theta,\chi\right) = -\sum_{n=-\infty}^{\infty} \frac{\pi}{(1-M_\infty^2\sin^2\chi)^{\frac{1}{2}}} \exp\left\{in\left[\frac{\omega R}{v(\chi)}+\theta\right]\right\}\mu(n,k_s), \tag{3.11b}$$

$$v(\chi) = U_\infty\cos\chi + (a_\infty^2 - U_\infty^2\sin^2\chi)^{\frac{1}{2}}, \tag{3.11c}$$

and k_s is the stationary phase point ($k = k_s$) given by

$$k_s = \frac{\omega n}{a_\infty}\left[\frac{\cos\chi}{(1-M_\infty^2\sin^2\chi)^{\frac{1}{2}}} - M_\infty\right]\frac{1}{1-M_\infty^2}. \tag{3.12}$$

3.1. *Thickness noise*

For the thickness-noise problem it is easy to find upon substituting the right-hand side of (2.17) for $f(r, \theta, z)$ the following formula for $\mu(n, k_s)$ of (3.11),

$$\bar{f}_n(r, k_s) = \sum_{m=1}^{B} \frac{\rho_\infty}{2\pi^2} \int_0^{2\pi} \int_{-\infty}^{\infty} \left[\left(U_\infty \frac{\partial}{\partial z} - \omega \frac{\partial}{\partial \theta} \right) (U_\infty^2 + \omega^2 r^2)^{\frac{1}{2}} \frac{\partial h}{\partial \xi_m} \delta(\zeta_m) \right] \times \exp\{-\mathrm{i}(k_s z + n\theta)\} \, \mathrm{d}z \, \mathrm{d}\theta, \quad (3.13)$$

$$\mu_T(n, k_s) = \int_0^b \bar{f}_n(r, k_s) \exp\{-\tfrac{1}{2} n\pi \mathrm{i}\} J_n\left(\frac{\omega n \sin\chi}{a_\infty (1 - M_\infty^2 \sin^2\chi)^{\frac{1}{2}}} r \right) r \, \mathrm{d}r, \quad (3.14)$$

where J_n = Bessel function of order n. The subscript T in (3.14) denotes the thickness-noise component. To evaluate the double integral of (3.13) it is advantageous to perform an integration by parts on z and θ first. This effectively replaces the operator $(U_\infty(\partial/\partial z) - \omega(\partial/\partial\theta))$ in the integrand by the factor $\mathrm{i}(U_\infty k_s - \omega n)$. After integration by parts the double integration can be carried out by changing the integration variables from $r \, \mathrm{d}z \, \mathrm{d}\theta$ to $\mathrm{d}\zeta_m \, \mathrm{d}\xi_m$. Both integrations cover the same curve surface of the circular cylinder of radius r. On substituting z and θ of the exponential function of the integrand of (3.13) by the expressions given in (2.10), the integral over the delta function $\delta(\zeta_m)$ can readily be evaluated giving

$$\bar{f}_n(r, k_s) = \sum_{m=1}^{B} \frac{\mathrm{i}\rho_\infty}{2\pi^2} \frac{U_\infty k_s - \omega n}{r} (U_\infty^2 + \omega^2 r^2)^{\frac{1}{2}} \exp\{-\mathrm{i}(k_s \eta + n\theta_m)\} \times \int_{\text{chord}} \frac{\partial h}{\partial \xi_m} \exp\left\{ \mathrm{i} \left[\frac{U_\infty k_s - \omega n}{(U_\infty^2 + \omega^2 r^2)^{\frac{1}{2}}} \right] \xi_m \right\} \mathrm{d}\xi_m. \quad (3.15)$$

The integral which appears as the last factor of (3.15) has the same value for all the blades. Further, since the thickness function of the airfoil sections used for turbopropeller blades are polynomials (or can be closely approximated by polynomials) the integral can be determined in closed form. To display the sweep of the blade explicitly a change of integration variables from ξ_m to t is made, see figure 5. These variables are related by

$$\xi_m = x_C - D(r) - t, \quad (3.16)$$

where x_C is the distance between the leading edge of the blade and the centre of gravity of the airfoil section. This leads to

$$\int_{\text{chord}} \frac{\partial h}{\partial \xi_m} \exp\left\{ \mathrm{i} \left[\frac{U_\infty k_s - \omega n}{(U_\infty^2 + \omega^2 r^2)^{\frac{1}{2}}} \right] \xi_m \right\} \mathrm{d}\xi_m = -\int_0^C \frac{\partial h(t, r)}{\partial t} \exp\left\{ \mathrm{i} \left[\frac{U_\infty k_s - \omega n}{(U_\infty^2 + \omega^2 r^2)^{\frac{1}{2}}} \right] (x_C - D - t) \right\} \mathrm{d}t, \quad (3.17)$$

where C is the chord width.

Now the blades of the turbopropeller are spaced at equal intervals so that without loss of generality θ_m may be taken to be

$$\theta_m = \frac{2\pi(m-1)}{B}. \quad (3.18)$$

The summation over m of (3.15) may easily be carried out by noting that

$$\sum_{m=1}^{B} \exp\left\{ -\mathrm{i} \frac{2n(m-1)}{B} \right\} = \begin{cases} B & (n = 0, \pm B, \pm 2B, \ldots), \\ 0 & (\text{otherwise}). \end{cases}$$

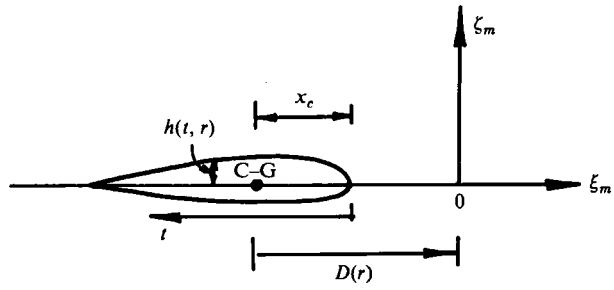

FIGURE 5. Airfoil section of turbopropeller blade, $\xi_m = -D + x_c - t$.

It follows, therefore, $\bar{f}_n$ of (3.15) is zero unless n is equal to an integral multiple of B, i.e. $n = NB$ where N is an integer. Hence

$$\bar{f}_n(r, k_s) = -\frac{iB\rho_\infty}{2\pi^2 r}(U_\infty k_s - \omega n)(U_\infty^2 + \omega^2 r^2)^{\frac{1}{2}} \times \exp\left\{-i\left[k_s \eta + \frac{U_\infty k_s - \omega n}{(U_\infty^2 - \omega^2 r^2)^{\frac{1}{2}}}(D - x_C)\right]\right\} \int_0^C \frac{\partial h(t, r)}{\partial t} \times \exp\left\{-i\left[\frac{U_\infty k_s - \omega n}{(U_\infty^2 + \omega^2 r^2)^{\frac{1}{2}}}\right] t\right\} dt\, \delta_{n, NB} \quad (\delta_{n, NB} = \text{Kronecker delta}). \tag{3.19}$$

From (3.19) it can be seen that, because of the blade sweep $D(r)$ and the phase alignment $\eta(r)$, two-phase factors are introduced into the solution. These phase factors when integrated over r result in rapid cancellation of the radiated noise as was noted previously by Hanson (1980*a*, *b*). Equations (3.19), (3.14) and (3.11) constitute the solution of the thickness-noise problems. They will be used for numerical computation in §6.

3.2. *Loading noise*

For the loading-noise problem the inhomogeneous term of (3.1) is given by that of (2.19). On proceeding as in the case of thickness noise it is straightforward to find that the corresponding formulas for the loading noise are (subscript L denotes loading noise)

$$\mu_L(n, k_s) = \int_0^b \bar{F}_n(r, k_s) \exp\{-\tfrac{1}{2}n\pi i\} J_n\left(\frac{\omega n \sin\chi}{a_\infty (1 - M_\infty^2 \sin^2\chi)^{\frac{1}{2}}} r\right) r\, dr, \tag{3.20}$$

where

$$\bar{F}_n(r, k_s) = \frac{iB}{4\pi^2}\left(k_s \omega + \frac{U_\infty n}{r^2}\right) \frac{1}{(U_\infty^2 + \omega^2 r^2)^{\frac{1}{2}}} \exp\left\{-i\left[k_s \eta + \frac{(U_\infty k_s - \omega n)}{(U_\infty^2 + \omega^2 r^2)^{\frac{1}{2}}}(D - x_C)\right]\right\} \times \int_0^b L(t, r) \exp\left\{-i\left(\frac{U_\infty k_s - \omega n}{(U_\infty^2 + \omega^2 r^2)^{\frac{1}{2}}}\right) t\right\} dt\, \delta_{n, NB}. \tag{3.21}$$

The total noise field generated by the turbopropeller is the sum of the thickness noise and the loading noise. Quantitatively it is given by replacing $\mu(n, k_s)$ in (3.11) by the algebraic sum of μ_T and μ_L, that is,

$$\mu(n, k_s) = \mu_T(n, k_s) + \mu_L(n, k_s). \tag{3.22}$$

The μs are complex quantities so that the two noise components may reinforce or cancel each other depending on their relative phases. Clearly, from (3.11) the

magnitudes of the Nth blade-passing harmonic of the total, thickness and loading noise are given by $2^{\frac{1}{2}}\pi/R(1-M_\infty^2\sin^2\chi)^{\frac{1}{2}}$ multiplies the absolute values of μ, μ_T and μ_L with $n = NB$ respectively. Thus to find the spectrum of turbopropeller noise it is only necessary to compute the absolute values of μ at all the blade-passing harmonics.

4. Nonlinearization

The acoustic field generated by an advanced turbopropeller as given by (3.11) has the form

$$p(R,\chi,\theta) = \frac{1}{R}F\left(\frac{\omega R}{v(\chi)}+\theta,\chi\right), \tag{4.1a}$$

where

$$v(\chi) = U_\infty\cos\chi+(a_\infty^2-U_\infty^2\sin^2\chi)^{\frac{1}{2}}. \tag{4.1b}$$

On replacing θ by $(\theta_s-\omega t)$, see (2.7), it is readily seen that the quantity $v(\chi)$ has the physical meaning of being the radial propagation velocity of the acoustic disturbances at a polar angle χ (in the stationary or non-rotating coordinate system). This propagation velocity is determined by the speed of sound, a_∞, and the convection velocity of the free-stream fluid, U_∞. In (3.11) the quantity $v(\chi)$ was derived by the method of stationary phase. In order to gain a better insight into why the propagation velocity of acoustic disturbance is given by (4.1b), here it will be rederived by purely geometrical and physical reasonings.

Consider an acoustic disturbance which in the absence of the uniform flow, U_∞, would be propagating radially in a direction with polar angle $(\chi+\nu)$. In the plane containing the radial vector at polar angle $(\chi+\nu)$ and the z-axis the velocity-vector diagram for the acoustic disturbance is as shown in figure 6. Because of the convection velocity U_∞ the acoustic disturbance will not be propagating radially in the direction $(\chi+\nu)$. Instead it will propagate in the direction χ. From figure 6 it is easy to find in the velocity diagram $AB = U_\infty\cos\chi$ and $AO = (a_\infty^2-U_\infty^2\sin^2\chi)^{\frac{1}{2}}$. Hence the resultant radial propagation velocity, $v(\chi) = OB$, is $v(\chi) = U_\infty\cos\chi+(a_\infty^2-U_\infty^2\sin^2\chi)^{\frac{1}{2}}$ in agreement with the result obtained by the method of stationary phase.

Now if weakly nonlinear propagation effects are to be included the speed of propagation of the acoustic disturbance in the radial direction will be slightly modified. The principal effects that are to be accounted for are:

(i) change in the speed of sound due to compression or rarefaction associated with the acoustic disturbance;

(ii) increase or decrease in propagation speed due to fluid-particle velocity induced by the acoustic disturbance.

To calculate these two effects let $a = a_\infty+a'$ be the speed of sound. The first-order correction a' can be determined from the isentropic flow relation. Thus

$$a' = \frac{\gamma-1}{2}\frac{p}{\rho_\infty a_\infty}. \tag{4.2}$$

where γ is the ratio of specific heats. On replacing a_∞ by $(a_\infty+a')$ in figure 6, it is easy to see that the change in the propagation velocity of the acoustic disturbance in the radial direction, v', is equal to

$$v' = a'\cos\nu = \frac{\gamma-1}{2}\frac{p}{\rho_\infty a_\infty}(1-M_\infty^2\sin^2\chi)^{\frac{1}{2}}. \tag{4.3}$$

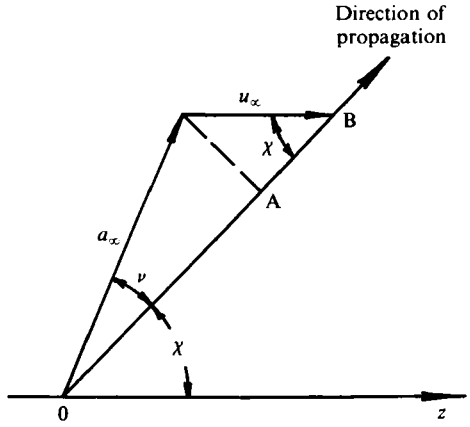

FIGURE 6. Velocity vector diagram in a plane containing the z-axis.

The fluid-particle velocity induced by the acoustic disturbance in the radial direction, to the first order, is $\partial\Phi/\partial R$. In the far field Φ has the same functional form as p, i.e.

$$\Phi = \frac{1}{R}\bar{\Phi}\left(\frac{\omega R}{v(\chi)} + \theta, \chi\right) \quad (R \gg b). \tag{4.4}$$

On substituting (4.4) into (2.4) it is straightforward to find

$$\frac{\partial\Phi}{\partial R} = (1 - M_\infty^2 \sin^2\chi)^{\frac{1}{2}} \frac{p}{\rho_\infty a_\infty} \quad (R \gg b). \tag{4.5}$$

By combining (4.3) and (4.5) the change in radial propagation velocity, Δv_{R}, due to both effects in terms of the far-field pressure p is

$$\Delta v_{\mathrm{R}} = \tfrac{1}{2}(\gamma+1)(1 - M_\infty^2 \sin^2\chi)^{\frac{1}{2}} \frac{p}{\rho_\infty a_\infty}. \tag{4.6}$$

To incorporate Δv_{R} into solution (4.1) the nonlinearization procedure of Whitham (1974) (chapter 9) will be adopted here. For a fixed direction χ the nonlinearized form of (4.1), following Whitham's method, is

$$p(R, \chi, \theta) = \frac{1}{R} F(\tau, \chi), \tag{4.7}$$

where $\tau(R, \theta, \chi)$ is to be determined from the improved characteristics. Including first-order effects, the radial propagation velocity is

$$-\omega \frac{\mathrm{d}R}{\mathrm{d}\theta} = v(\chi) + \Delta v_{\mathrm{R}}. \tag{4.8}$$

On using the expression of (4.6) for Δv_{R}, (4.8) may be rewritten as

$$\frac{\mathrm{d}\theta}{\mathrm{d}R} \simeq \frac{-\omega}{v(\chi)}\left[1 - \tfrac{1}{2}(\gamma+1)\frac{(1 - M_\infty^2 \sin^2\chi)^{\frac{1}{2}}}{v(\chi)} \frac{p}{\rho_\infty a_\infty}\right]. \tag{4.9}$$

In (4.9) the form of p is given by (4.7). Hence, upon integration with respect to R the improved characteristics

$$\theta = -\frac{\omega R}{v(\chi)} + \tfrac{1}{2}(\gamma+1)\frac{(1 - M_\infty^2 \sin^2\chi)^{\frac{1}{2}}}{v^2(\chi)} \frac{\omega}{\rho_\infty a_\infty} F(\tau, \chi) \ln\left(\frac{R}{b}\right) + \tau, \tag{4.10}$$

are found. In deriving (4.10) it has been assumed that at the tip of the blade, $R = b$, the linear solution applies. The implicit solution (4.7) and (4.10), obtained after eliminating τ, constitutes the nonlinearized solution.

5. Shock fitting

It is well known that nonlinearized solutions of the form of (4.7) and (4.10) most probably would lead to non-uniqueness of solutions as the nonlinearized acoustic disturbances evolve in space and time. In order to remove the degeneracy it is necessary to include weak shocks as a part of the solution. For each value of τ, (4.10) gives a characteristic curve in the (θ, R)-plane. A shock will form when some of these characteristics intersect or overlap each other. The formation of a shock usually begins when two neighbouring characteristics start to touch each other to form an envelope. Consider two neighbouring characteristics τ and $\tau+\delta\tau$. Suppose they touch each other at $\theta = \theta_s$ and $R = L_s$ (L_s is the shock formation distance; see figure 7); then from (4.10) these characteristics satisfy the following relations:

$$\theta_s = -\frac{\omega L_s}{v(\chi)} + \tfrac{1}{2}(\gamma+1)\frac{(1-M_\infty^2\sin^2\chi)^{\frac{1}{2}}}{v^2(\chi)}\frac{\omega}{\rho_\infty a_\infty}F(\tau,\chi)\ln\left(\frac{L_s}{b}\right)+\tau, \tag{5.1}$$

$$\theta_s = -\frac{\omega L_s}{v(\chi)} + \tfrac{1}{2}(\gamma+1)\frac{(1-M_\infty^2\sin^2\chi)^{\frac{1}{2}}}{v^2(\chi)}\frac{\omega}{\rho_\infty a_\infty}F(\tau+\delta\tau,\chi)\ln\left(\frac{L_s}{b}\right)+\tau+\delta\tau. \tag{5.2}$$

Upon expanding (5.2) for small $\delta\tau$ and subtracting (5.1) from it, one finds to order $\delta\tau$

$$\left[\tfrac{1}{2}(\gamma+1)\frac{(1-M_\infty^2\sin^2\chi)^{\frac{1}{2}}}{v^2(\chi)}\frac{\omega}{\rho_\infty a_\infty}\frac{\partial F}{\partial\tau}\ln\left(\frac{L_s}{b}\right)+1\right]\delta\tau = 0. \tag{5.3}$$

Hence on equating the terms in the square bracket to zero a formula for the shock-formation distance is obtained,

$$\frac{L_s}{b} = \exp\left[\frac{2}{\gamma+1}\frac{v^2(\chi)\rho_\infty a_\infty}{(1-M_\infty^2\sin^2\chi)^{\frac{1}{2}}\omega}\frac{1}{(-\partial F/\partial\tau)_{\max}}\right]. \tag{5.4}$$

Beyond the shock-formation distance i.e. for $R > L_s$, the shock surfaces are three-dimensional. However, because $F(\tau,\chi)$ is periodic in τ with period $2\pi/B$ it is, therefore, only necessary to confine attention to the shocks in a single period, that is, the shocks associated with one of the blades of the turbopropeller. To construct the three-dimensional shock surfaces the simplest approach is to select a direction χ and consider the evolution of the acoustic disturbances and shock waves in the radial direction R as time t increases or as θ decreases. The primary advantage of this approach is that for a fixed χ the shock-fitting procedure can be carried out relatively easily in the (R,θ)-plane. After the shocks are determined for the selected direction χ, the shock-fitting procedure can be repeated for a new value of χ. Thus by varying χ over an appropriate range of angles the development of the shock surfaces in space and time can be determined.

Whitham (1974) outlined in detail how weak shocks can be fitted into a weakly nonlinearized solution. For a fixed χ, let τ_1 and τ_2 be the characteristics on the two sides of the shock in the (R,θ)-plane. It can readily be shown following Whitham that the equal-area rule, namely

$$\tfrac{1}{2}[F(\tau_1,\chi)+F(\tau_2,\chi)](\tau_1-\tau_2) = \int_{\tau_1}^{\tau_2}F(\tau,\chi)\,d\tau, \tag{5.5}$$

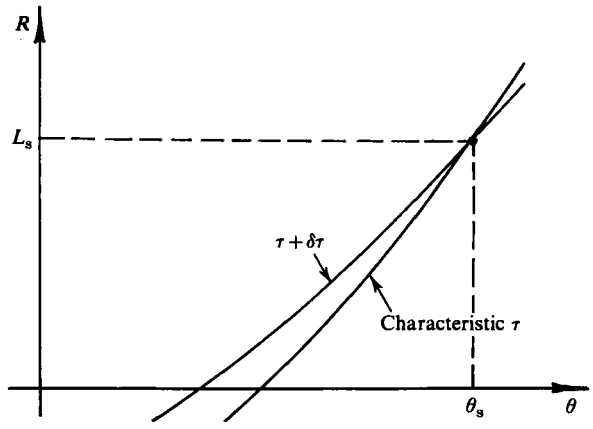

FIGURE 7. The (R, θ)-plane showing characteristics τ and $\tau+\delta\tau$ and the shock-formation distance.

is applicable to the present problem. Equation (5.5) together with the two characteristic equations for τ_1 and τ_2 (see (4.10)) permit the determination of τ_1, τ_2 and the time of arrival of the shock, $\theta_s(R)$, at any radial distance R ($R > L_s$). This information when incorporated into the nonlinearized solution of (4.7) and (4.10) provides the nonlinearized waveform (with shocks) of the acoustic disturbance as would be measured by an observer at (R, χ). Numerical results illustrating the steepening of the waveform into shocks and their subsequent spatial evolution in the radial direction will be provided and discussed in the next section.

6. Numerical results and comparison with experiment

In §3, explicit formulas for the thickness and loading noise generated by a turbopropeller, according to linear acoustic theory, were derived. The solution to the thickness-noise problem is given by (3.19), (3.14) and (3.11). To calculate this noise component the first step is to input the geometry of the blades through (3.19). It turns out for the SR-3 propfan that the blade-thickness distribution $h(t, r)$ at any radial location r has a simple polynomial representation in t plus a square-root t term for the leading edge. On substituting this representation of h into (3.19) the integral there may be evaluated analytically. The next step in the calculation is to use this analytical expression of $\bar{f}_n$ to determine the complex amplitude of the Nth blade-passing harmonic, $\mu_T(N, k_s)$, for a given direction of noise radiation, χ, according to (3.14). The integrand as a function of r of the integral in this equation is very complicated. However, it can easily be computed numerically. In the integrand, the Bessel function is highly oscillatory when N is large or for the higher harmonics. To ensure sufficient numerical accuracy in the integration, the size of the integration step is taken to vary with N so that there are at least twenty steps within one period of oscillation. The Bessel functions J_n are generated following the procedure described in a paper by Tam (1983). The solution of the loading-noise problem is given by (3.21), (3.20) and (3.11). The computation of this noise component is carried out in a similar manner to the thickness noise. To obtain the waveform (pressure–time history) of the turbopropeller noise, the complex amplitudes of the different blade-passing harmonics of the thickness and loading noise are first combined according to (3.22). The summation over n in (3.11*b*) is then carried out using the method of fast Fourier

transform in much the same way as discussed by Tam (1983). A computer program implementing all the above computation steps has now been developed. The input to the computer program consist of the cruise Mach number (U_∞/a_∞), the blade-tip rotational Mach number ($\omega b/a_\infty$, where b is the length of the blades), the geometry of the blades and the loading distribution on the blades. For a specified direction of radiation, χ, the program computes the thickness, the loading and the total noise spectra as well as the pressure waveform.

To incorporate the weakly nonlinear propagation effects into the numerical solution the nonlinearized characteristic (4.10) is used. In this equation the waveform function $F(\tau, \chi)$ is calculated according to the linear acoustic theory described above. To determine the nonlinearized pressure waveform at a given distance R ($R > b$) the relationship $\theta(\tau)$ is computed by (4.10). Since $F(\tau, \chi)$ is already known, the nonlinearized waveform $F(\theta, \chi)$ is obtained. For R greater than the shock-formation distance, the nonlinearized waveform is multivalued. To reduce the waveform to a single-valued function a weak shock is fitted in the nonlinear waveform following the procedure described in §5. A simple way to implement the shock-fitting criteria is to first compute the slope of the chord joining the two characteristics τ_1, τ_2 which mark the two sides of the shock. On using (4.10) it is straightforward to find

$$\frac{F(\tau_2, \chi) - F(\tau_1, \chi)}{\tau_2 - \tau_1} = \frac{-v^2(\chi)\rho_\infty a_\infty}{\frac{1}{2}(\gamma+1)(1-M_\infty^2 \sin^2\chi)^{\frac{1}{2}}\omega \ln(R/b)}. \tag{6.1}$$

Since the right-hand side of (6.1) is known, this equation provides a simple relationship between τ_1 and τ_2. To determine τ_1 numerically the value of τ_1 is adjusted by small increments until the equal-area rule of (5.5) is satisfied. On substituting this value of τ_1 into the nonlinear characteristic (4.10), the time of arrival of the shock during a typical blade-passing period at a given radial and angular position can be easily calculated.

Before comparing the present calculated results, including weakly nonlinear propagation effects, with the JETSTAR measurements (see Brooks 1983) it is worthwhile emphasizing that, whereas no ambiguity exists in the determination of the thickness noise since the input of this noise component depends on the propfan blade geometry alone, the same is not true for the loading noise. At the present time the loading on the SR-3 propfan can, at best, be estimated. A semi-empirical lift-coefficient distribution (suggested by the manufacturer; Hanson, private communication) as a function of radial distance is used in the present calculation. In the work of Hanson (1980*a*, *b*) the chordwise loading distribution was assumed to be parabolic and symmetric with zero loading at the leading and trailing edge of the blade. It turns out for the SR-3 propfan operating at the design condition with cruise Mach number 0.8 and blade-tip rotational Mach number 0.825, the thickness noise is the more dominant component. Because of this the uncertainty in the loading distribution introduces only a relatively minor (although not negligible) effect on the predicted results. To test the sensitivity of the predicted noise characteristics to the form of chordwise loading distribution, the noise spectra of the SR-3 propfan at cruise condition at 30000 feet altitude have been calculated for two assumed forms of distribution. Figure 8 shows the results at $\chi = 73°$ at an observation distance of 2.6 blade length (this is the design distance to the aircraft fuselage). The spectrum indicated by the lighter lines corresponds to a symmetric parabolic chordwise distribution. The spectrum indicated by the heavy dark lines corresponds to a linear chordwise distribution. In the linear chordwise loading-distribution model, the loading is assumed to be maximum at the leading edge of the blade and decreases

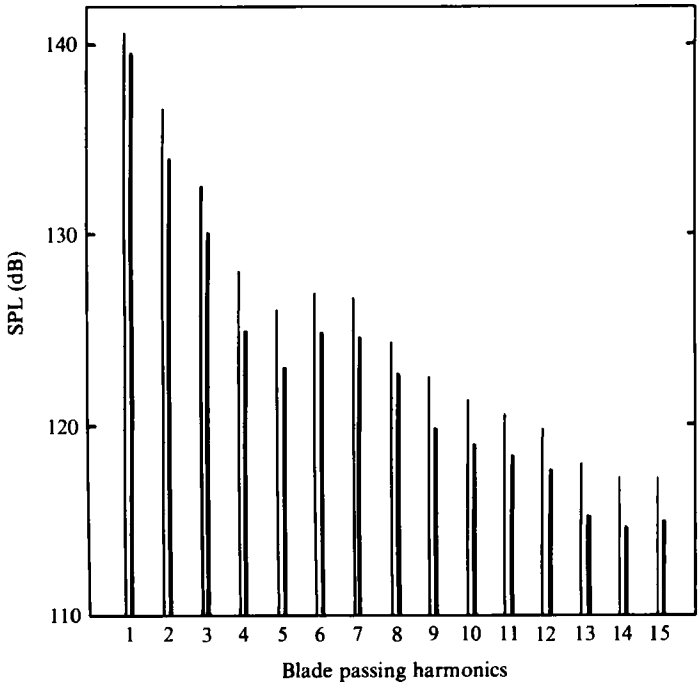

FIGURE 8. Spectrum of the total noise for the SR-3 propfan at cruise condition at 30000 feet altitude; $R = 2.6$ blade length; $\chi = 73°$; chordwise loading distribution: ——, parabolic; ——, linear.

to zero at the trailing edge for radial locations up to where the free-stream helical Mach number is equal to 0.9. Such a distribution should be a reasonably good approximation in the subsonic part of the blade. At the tip of the blade the helical Mach number is supersonic. Here the chordwise loading distribution is assumed to be uniform over the whole chord. In the region between the triangular and the uniform distribution the chordwise distribution is assumed to change linearly in the radial direction from one form to the other. As can be seen, for the direction $\chi = 73°$ the parabolic chordwise loading distribution gives higher pressure amplitudes for all the first fifteen blade-passing harmonics shown in figure 8. Figure 9 shows a comparison of the corresponding waveforms. It is clear that the major difference between the two waveforms lies in the magnitude of the negative pressure peak. The difference is not completely negligible. It is interesting to point out that this difference cannot be realized if one restricts one's attention to the spectrum and especially to the fundamental blade-passing harmonic alone as is often done. In this case the difference between the fundamental blade harmonic is only 1.1 dB.

At $\chi = 90°$ on the other hand, the calculated waveform appears to be not as sensitive to the chordwise loading distribution. Figure 10 shows the calculated waveform at this angle at the fuselage for the linear as well as the parabolic chordwise loading distribution. The gross features of the two waveforms do not differ greatly. Figure 11 shows the nonlinearized waveform. Again the gross features of the nonlinearized waveforms (with a shock) are nearly identical. In fact, experience indicates that for a wide range of angle χ the nonlinearized waveform is not very sensitive to the assumed form of chordwise loading distribution. With the above information it is believed that a comparison between calculated results and the

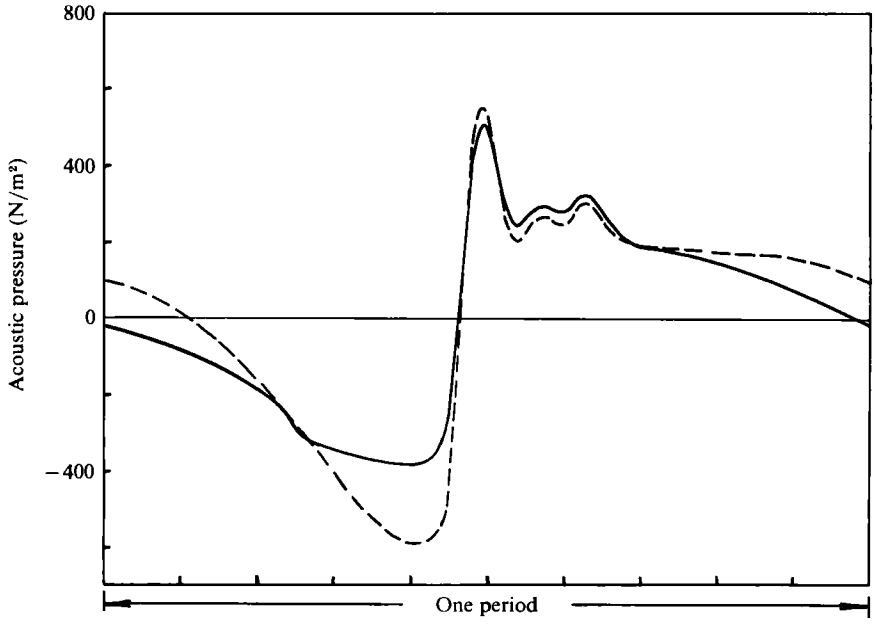

FIGURE 9. Pressure waveform of the noise of SR-3 propfan according to linear theory; $\chi = 73°$; chordwise loading distribution: ----, parabolic; ——, linear.

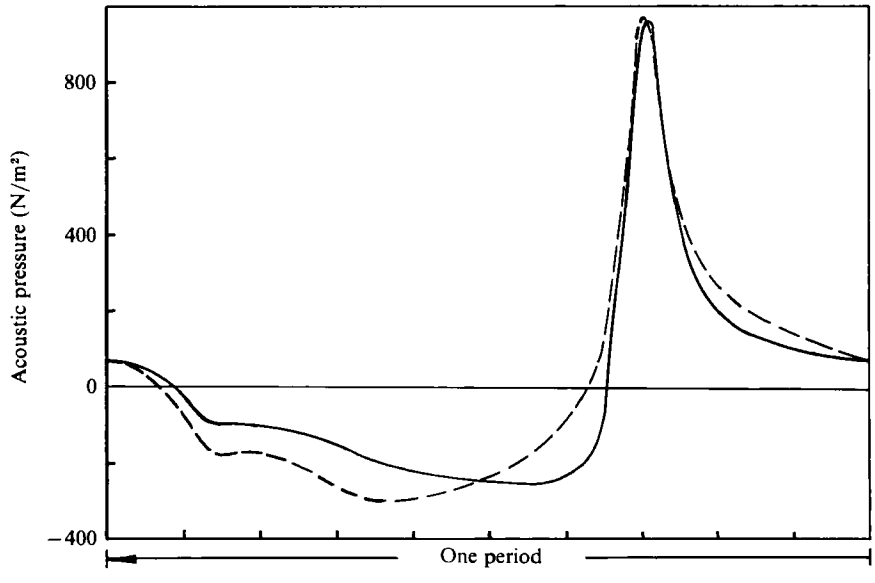

FIGURE 10. Pressure waveform of the noise of SR-3 propfan according to linear theory; $\chi = 90°$; chordwise loading distribution: ----, parabolic; ——, linear.

JETSTAR flight measurements at the $\chi = 90°$ direction constitutes a very reliable test of the validity of the theory. The comparison is shown in figure 12. The waveform of the JETSTAR measurements is taken from the report by Brooks (1983) (only the pressure measurements from the microphones mounted on the boom which are not shielded by the fuselage boundary layer are used in comparison with calculated

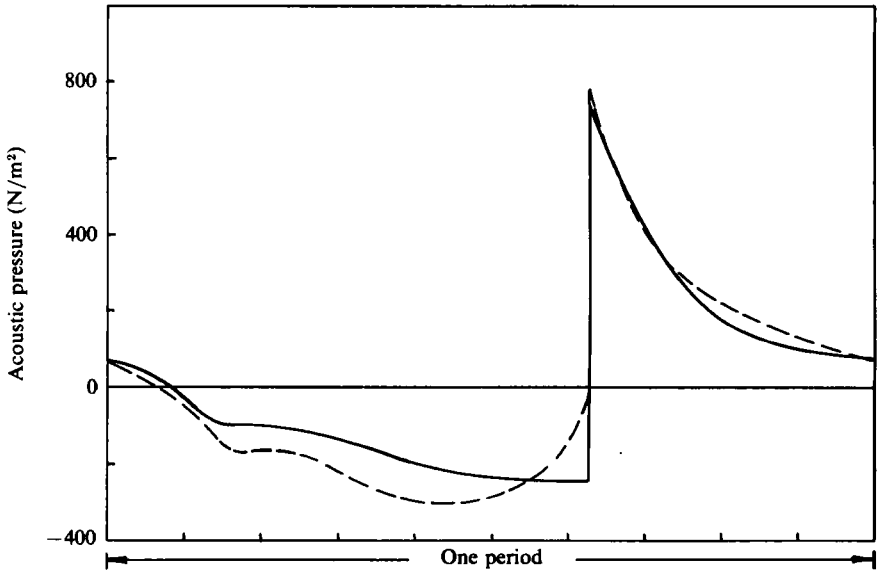

FIGURE 11. Nonlinearized pressure waveform of the noise of SR-3 propfan; $\chi = 90°$; chordwise loading distribution: ----, parabolic; ——, linear.

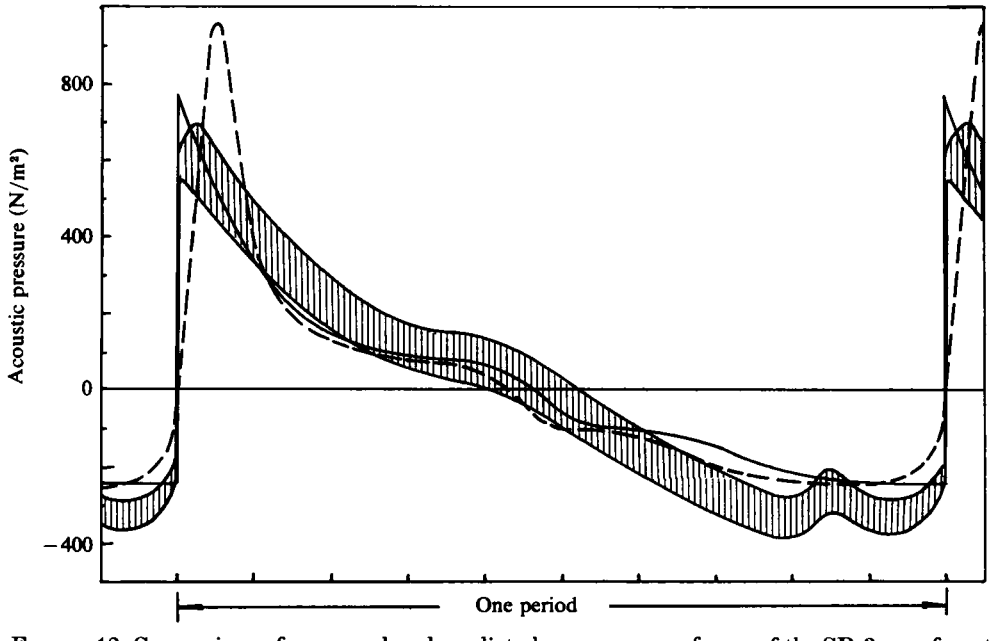

FIGURE 12. Comparison of measured and predicted pressure waveforms of the SR-3 propfan at the cruise condition at 30000 feet altitude; $\chi = 90°$; $R = 2.6$ blade length; ---, linear theory; ——, weakly nonlinear theory; shaded area, JETSTAR measurements (superposition of five sweeps of the oscilloscope).

results). The measured waveform is a combination of five sweeps on the oscilloscope. The dotted curve in the figure is the waveform according to the linear theory. The full curve is the nonlinearized solution with a weak shock fitted according to the equal-area rule. From the figure it can be seen that the linear theory (linear chordwise

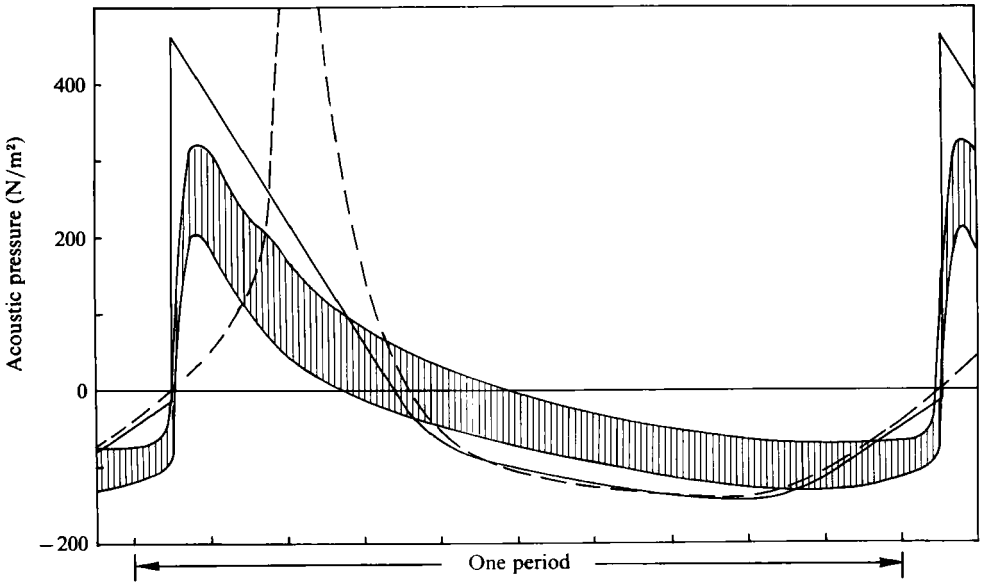

FIGURE 13. Comparison of measured and predicted pressure waveforms of the SR-3 propfan at the cruise condition at 30000 feet altitude; $\chi = 110°$; $R = 2.6$ blade length; – – –, linear theory; ——, weakly nonlinear theory; shaded area, JETSTAR measurements (superposition of five sweeps of the oscilloscope).

loading distribution assumed) not only fails to predict the measured shock wave but also over-predicts the maximum magnitude of the acoustic pulse. The weakly nonlinear results, on the other hand, agree reasonably well with the measurement. The steepening of the pressure pulse into a weak shock is correctly predicted. The calculated maximum positive pressure at the back of the shock also agrees better with the data than that of the linear theory, indicating that weakly nonlinear propagation effects should be taken into account for accurate supersonic turbopropeller noise prediction.

Figures 13 and 14 show the calculated and the measured pressure waveforms of the Boom 1 ($\chi = 110°$) and Boom 4 ($\chi = 73°$) microphone of the JETSTAR flight experiment. The Boom 1 microphone was mounted in the upstream or forward quadrant of the turbopropeller while the Boom 4 microphone was located in the aft quadrant. As can be readily seen both measured pressure waveforms are characterized by a shock wave. In the forward quadrant the waveform appears to bear a strong resemblance to the classical N-wave signature familiar in the sonic boom phenomenon. The indication is that nonlinear effects have exerted a stronger influence on the shape of the acoustic pulses radiated in the forward direction than on those radiated in the aft direction. On comparing the calculated results and measurements it is easy to see that there is very favourable overall agreement between the weakly nonlinear theory (with shocks fitted in the solution) and experiment. In the forward direction, the theoretical waveform has a nearly N-wave profile immediately after the shock very similar to the measured data. The maximum positive pressure just behind the shock is, however, overpredicted. In figure 13 the calculated waveform of the linear theory is also shown (the dotted curve). It is clear that this waveform does not compare as well with the measurement, again reinforcing the belief that nonlinear propagation effects cannot be neglected. In the aft direction, figure 14, the difference between the

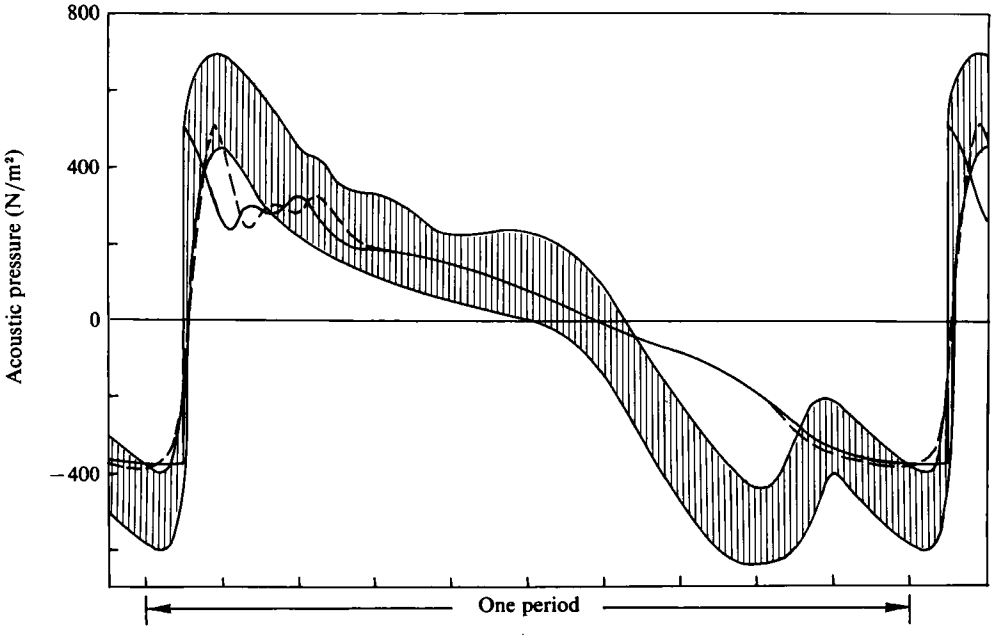

FIGURE 14. Comparison of measured and predicted pressure waveforms of the SR-3 propfan at the cruise condition at 30000 feet altitude; $\chi = 73°$; $R = 2.6$ blade length; ---, linear theory; ——, weakly nonlinear theory; shaded area, JETSTAR measurements (superposition of five sweeps of the oscilloscope).

calculated waveforms based on the linear and the weakly nonlinear theories is small. Both appear to compare quite well with the observed data.

From the calculated and measured results (figures 13 and 14) it is evident that the importance of weakly nonlinear propagation effects on high-speed turbopropeller noise is a function of the direction of radiation. One way to obtain a rough idea of the directional dependence is to examine the shock-formation distance as a function of direction. The shock-formation distance due to weakly nonlinear propagation effects is given by (5.4). Figure 15 shows the calculated results for the SR-3 propfan operated at cruise condition. These results indicated that in the forward direction especially near $\chi = 110°$ the acoustic pulse from each blade steepens to form a shock almost immediately after propagating a short distance from the tip of the blade. In the aft directions the shock-formation distance is, however, much longer again, suggesting that weakly nonlinear propagation effects would not exert their influence as quickly as in the forward directions. From figure 15 it is to be noted that shock waves are, for all intents and purposes, confined to the sector $65° < \chi < 120°$. Outside this range the acoustic intensity is too weak to develop shocks.

Prior to the JETSTAR flight experiment the noise of the SR-3 propfan was measured at the open wind tunnel of the United Technology Research Center (UTRC) (see Brooks 1980; Brooks & Metzger 1980). The open wind tunnel, however, cannot be operated at high subsonic Mach number to match the design cruise condition. Because of this, the propfan was overspun so as to keep the helical-tip Mach number the same as the design value. It turns out the change in the cruise Mach number is not insignificant. One major consequence is that the pressure waveforms of this series of simulated tests are somewhat different from those obtained in the JETSTAR experiment. Nevertheless, these measured results provide a valuable independent set of supersonic

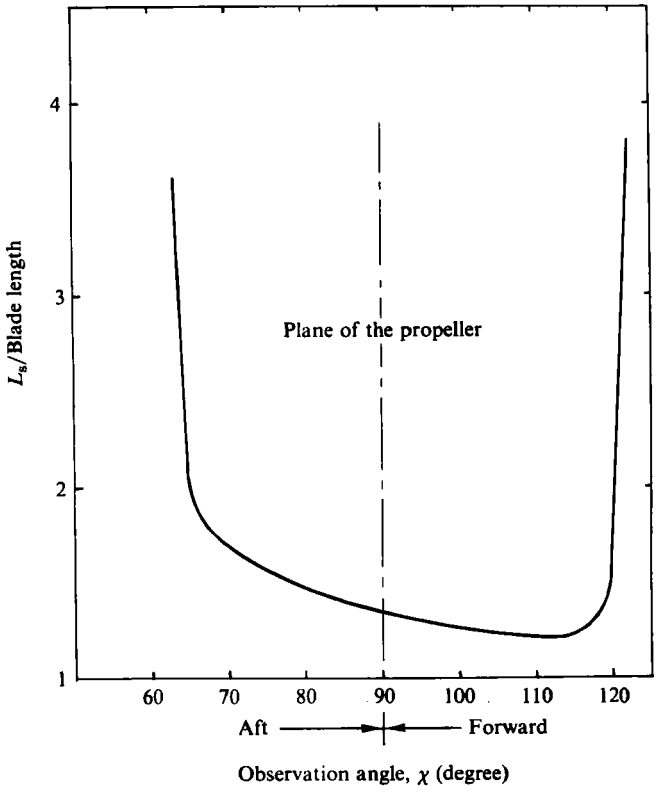

FIGURE 15. Shock-formation distance for the SR-3 propfan at cruise condition as a function of direction of radiation.

turbopropeller noise data for testing the present theory. Figures 16 and 17 show the measured pressure waveforms of two typical runs of the wind-tunnel data. Plotted in these figures also are the calculated pressure waveforms, with and without weakly nonlinear propagation effects. It is clear from the calculated results that at this low-cruise Mach number the weakly nonlinear effects are not very significant (at the distance of the design aircraft fuselage). Both calculated time-history curves compare quite well with the measurements for the two test conditions. The major deficiency in the theoretical results appears to be the overprediction of the maximum positive pressure amplitude. The widths of the pressure peaks are, however, correctly predicted.

In summary, comparisons between the computed results of the present theory and the JETSTAR flight data at a design cruise condition at 30000 feet altitude and the UTRC open wind tunnel low-cruise Mach number measurements have been made. Overall, reasonably good agreements are found in all cases. At low-cruise Mach number weakly nonlinear propagation effects are observed to be not very important at distance of the design aircraft fuselage. On the other hand, at high-subsonic-cruise Mach number nonlinear propagation effects lead quickly to the formation of shocks and strong distortion of the waveform. In the upstream or forward directions the pressure waveform immediately after the shock resembles the classical N-wave profile of the sonic boom phenomenon. It is found that weakly nonlinear propagation effects

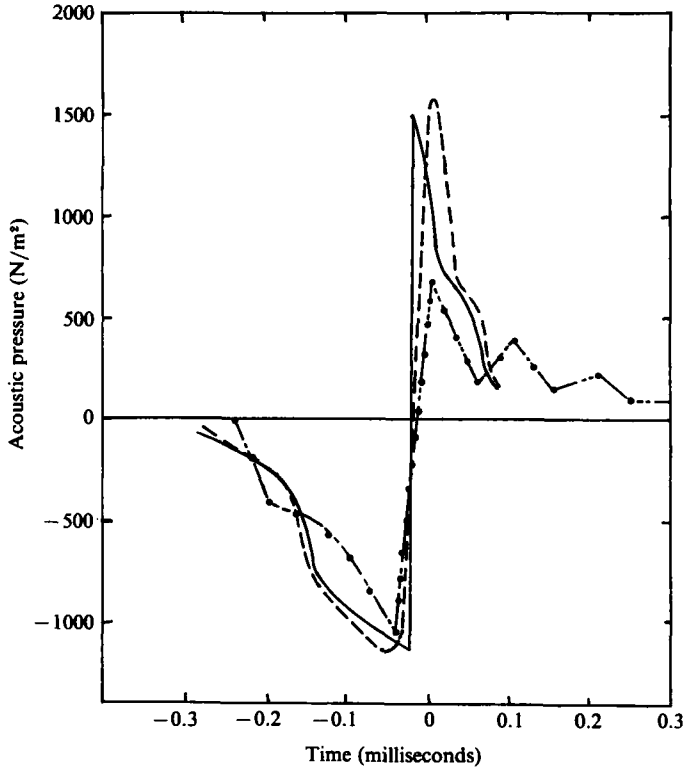

FIGURE 16. Comparison of measured and calculated results for 4-bladed SR-3 propfan; cruise Mach number = 0.323; RPM = 11300; $\chi = 93°$; $R = 2.6$ blade length; —●---●—, measurement (Brooks & Metzger 1980); ——, weakly nonlinear theory with shock; – – –, linear acoustic theory.

must be incorporated into the theory in order to bring the calculated results into close agreement with measurements. These effects, at the same distance from the propfan, are less pronounced in the aft directions.

7. Discussion

Let us now examine physically the conditions under which nonlinear propagation effects are important for turbopropeller noise. Obviously, nonlinear effect is important only if the noise intensity is sufficiently high. This is the case for supersonic turbopropeller. However, aside from the noise intensity one must recognize that nonlinear propagation effects are cumulative. That is to say, even a relatively weak effect when acting over a long period of time could result in an appreciable deformation of the waveform of the sound pulse associated with each blade. To allow enough time for weak nonlinearities to exert their cumulative influence it is sufficient that either the distance of propagation is long, or the effective speed of propagation is small, or both. For a turbopropeller, operating at the design condition, the effective velocity of propagation for acoustic disturbances (relative to the propeller) has been found to be given by (4.1*b*). Figure 18 shows a plot of this velocity normalized by the ambient speed of sound as a function of direction. It is easy to see that because of the free-stream convection velocity the propagation speed is small in the forward arc. In these directions the forward propagation velocity of the acoustic disturbances

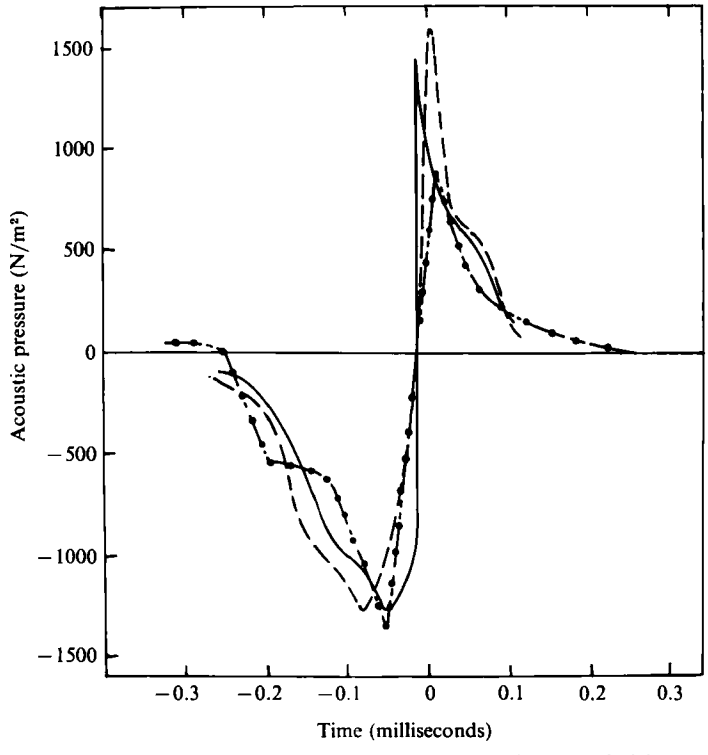

FIGURE 17. Comparison of measured and calculated results for 2-bladed SR-3 propfan; cruise Mach number = 0.323; RPM = 11 800; $\chi = 93°$; $R = 2.6$ blade length; —●----, measurement (Brooks & Metzger 1980); ——, weakly nonlinear theory with shock; ---, linear acoustic theory.

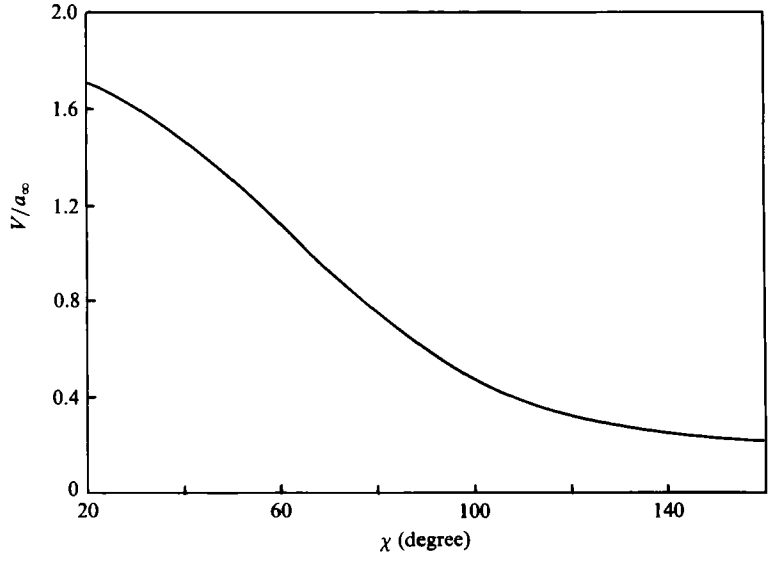

FIGURE 18. Calculated propagation velocity of acoustic disturbances in the blade-fixed coordinate system as a function of direction; $M_\infty = 0.8$.

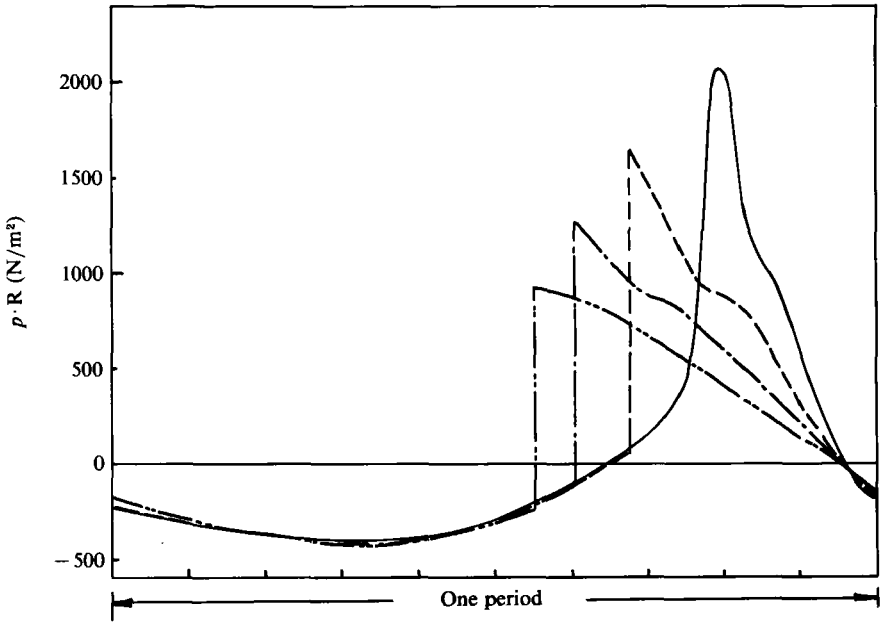

FIGURE 19. Calculated pressure waveforms of the noise of SR-3 propfan at $\chi = 110°$ and at an altitude of 30000 feet; ——, $R = 1$; – – –, $R = 2$; — — —, $R = 3$; — — — —, $R = 4$ (R in units of blade length).

is slowed down by the ambient flow. At $\chi = 90°$ the effective velocity is only 0.6 times the ambient speed of sound. Thus one would anticipate that the nonlinear propagation effect could be significant, at least, in the forward directions even for observation points that are close to the turbopropeller.

To illustrate the cumulative effect of weak nonlinearities in the propagation of turbopropeller noise, the space–time evolution of the pressure waveforms for the SR-3 propfan, in the direction $\chi = 110°$, is shown in figure 19. To focus our attention solely on this effect the value of pressure times R (i.e. pR) is plotted as a function of time in units of blade-passing period. The factor R is to account for the amplitude decay due to spherical divergence. In this direction calculation based on the present weakly nonlinear theory, indicates that a weak shock due to nonlinear propagation effect begins to form after the acoustic disturbance has propagated over a distance of about a fifth of the blade length measured from the blade tip. At a distance of two blade lengths, from the centre of the propfan, a well-defined shock, as shown in figure 19, is established. As the acoustic pulse continues to propagate, the positive part of the sound pulse quickly evolves into the classical N-shape configuration. The maximum pressure decreases continually as the radial distance increases. Based on the results shown in this figure it is clear that, for aircrafts with multiple-propeller system, the use of a weakly nonlinear turbopropeller-noise theory is necessary to obtain an accurate prediction of cabin-interior noise. This is especially so for the noise contributions from the outer propellers, since the noise from these propellers has to travel over a somewhat longer distance to reach the fuselage.

This work was supported by the Independent Research and Development program of the Lockheed–Georgia Company. The authors wish to thank Dr D. B. Hanson for valuable comments and suggestions on improving this paper.

REFERENCES

BARGER, R. L. 1980 Theoretical prediction of nonlinear propagation effects on noise signatures generated by subsonic or supersonic propellers or rotor blade tips. *NASA TP* 1660.

BROOKS, B. M. 1980 Acoustic measurements of three propfan models. *AIAA paper* 80-0995.

BROOKS, B. M. 1983 Analysis of JETSTAR propfan acoustic flight test data. *Hamilton Standard Engineering Report HSER* 8882.

BROOKS, B. M. & METZGER, F. B. 1980 Acoustic test and analysis of three advanced turboprop models. *NASA* CR-159667.

DUGAN, J. F., MILLER, B. A., GRABER, E. & SAGERSER, D. A. 1980 The NASA high-speed turboprop program. *NASA* TM 81561.

FARASSAT, F. 1975 Theory of noise generation from moving bodies with an application to helicopter rotors. *NASA* TR R-451.

FARASSAT, F. 1981 Linear acoustic formulas for calculation of rotating blade noise. *AIAA J.* **19**, 1122–1130.

FARASSAT, F. & SUCCI, G. P. 1980 A review of propeller discrete frequency noise prediction technology with emphasis on two current methods for time domain calculations. *J. Sound Vib.* **71**, 399–419.

FFOWCS WILLIAMS, J. E. & HAWKINGS, D. L. 1969 Sound generated by turbulence and surfaces in arbitrary motion. *Phil. Trans. Soc. Lond.* A **264**, 321–342.

GOLDSTEIN, M. E. 1976 *Aeroacoustics*. McGraw Hill, New York.

HANSON, D. B. 1980*a* Helicoidal surface theory for harmonic noise of propellers in the far field. *AIAA J.* **18**, 1213–1220.

HANSON, D. B. 1980*b* Influence of propeller design parameters on far field harmonic noise in forward flight. *AIAA J.* **18**, 1313–1319.

HANSON, D. B. 1985 Near-field frequency-domain theory for propeller noise. *AIAA J.* **23**, 499–504.

HANSON, D. B. & FINK, M. R. 1979 The importance of quadrupole sources in prediction of transonic tip speed propeller noise. *J. Sound Vib.* **62**, 19–38.

HAWKINGS, D. L. & LOWSON, M. V. 1974 Theory of open supersonic rotor noise. *J. Sound Vib.* **36**, 1–20.

JOU, W. H. 1979 Supersonic propeller noise in a uniform flow. *AIAA paper* 79-0348.

LIGHTHILL, M. J. 1952 On sound generated aerodynamically I – General theory. *Proc. R. Soc. Lond.* A **211**, 564–587.

METZGER, F. B. & ROHRBACH, C. 1979 Aeroacoustic design of the propfan. *AIAA paper* 79-0610.

NYSTROM, P. A. & FARASSAT, F. 1980 A numerical technique for calculation of the noise of high speed propellers with advanced geometry. *NASA* TP 1662.

TAM, C. K. W. 1983 On linear acoustic solutions of high speed helicopter impulsive noise problems. *J. Sound Vib.* **89**, 119–134.

TAM, C. K. W. & BURTON, D. E. 1984 Sound generated by instability waves of supersonic flows. Part I. Two dimensional mixing layers. Part II. Axisymmetric jets. *J. Fluid Mech.* **138**, 249–295.

WHITHAM, G. B. 1974 *Linear and nonlinear waves*. Wiley-Interscience, New York.

WOAN, C. J. & GREGOREK, G. M. 1978 The exact numerical calculation of propeller noise. *AIAA paper* 78-1122.